Engineering Fracture Mechanics 298 (2024) 109917

Contents lists available at ScienceDirect

Engineering Fracture Mechanics

journal homepage: www.elsevier.com/locate/engfracmech

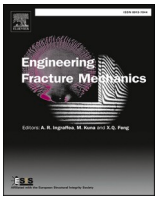

Mini-C(T) specimens for Master Curve analysis of structural steels operating within their ductile-to-brittle transition region

Marcos Sánchez *, Sergio Cicero, Borja Arroyo

LADICIM, Departamento de Ciencia e Ingeniería del Terreno y de los Materiales, University of Cantabria, Avenida de los Castros, 44, 39005 Santander, Spain

ARTICLE INFO

Keywords:
Mini-C(T)
Ductile-to-Brittle Transition Region
Reference Temperature
Master Curve
Structural Steels

ABSTRACT

This work uses mini-C(T) specimens, validated on nuclear steel grades, to characterize the fracture behavior of structural steels. Mini-C(T) specimens are significantly smaller (4 mm thick) than conventional fracture specimens and allow testing a large number of specimens with limited material. The research involves four common structural steels (S275JR, S355J2, S460M and S690Q), and involves testing, ASTM E1921 application and fractographical analyses. Findings demonstrate that mini-C(T) specimens effectively capture the fracture behavior of structural steels, providing reasonable T_0 values. Results show a difference of about ±30 °C comparing mini-C(T) and conventional specimens, suggesting the potential of mini-C(T) specimens for T_0 characterization.

1. Introduction

In recent years, specimen miniaturization has become very important in mechanical testing. There are many scenarios, within different engineering fields, where the use of conventional (large) specimens for structural integrity assessments becomes unfeasible for several reasons. This is the case in structural elements currently in service, where the removal of substantial portions of material is generally unattainable, such as in old bridges or reactor pressure vessels. Other typical situations where miniaturization of specimens may be of high interest are pipelines and welds, because of the complex geometries involved or the limited amount of available material. The use of small specimens, such as mini-tensile (e.g., [1–3]), Small Punch tests (e.g., [4–6]), or mini-C(T) specimens (e.g., [7–10]), offers a practical possibility to perform reliable structural integrity assessments.

Mini-C(T) specimens are 4 mm thick compact tension specimens based on the geometrical recommendations of the ASTM E1921 [11]. It is possible to obtain up to eight mini-C(T) specimens from a single broken Charpy specimen, something with important practical consequences in surveillance programs performed by the nuclear industry. In this context, the mini-C(T) testing approach brings numerous advantages, including: a) the direct evaluation of fracture toughness, rather than relying on semi-empirical approaches derived from Charpy measurements; b) the capacity to characterize the local properties of inhomogeneous materials; c) a significant increase of the number of specimens for monitoring, thereby increasing the material database and enhancing data reliability; d) a reduction in the amount of irradiated material required for testing; e) the possibility of changing the specimens' orientation (e.g., from T-L to L-T).

For metals with body-centered cubic (BCC) structures, such as ferritic-pearlitic steels, the material's fracture toughness experiences

* Corresponding author.
E-mail address: marcos.sanchez@unican.es (M. Sánchez).

https://doi.org/10.1016/j.engfracmech.2024.109917
Received 13 November 2023; Received in revised form 18 January 2024; Accepted 1 February 2024
Available online 8 February 2024

Table 1
Supply conditions of the structural steels [19–21].

Material	Minimum Yield Strength at room temperature (MPa)		Ultimate Tensile Strength at room temperature (MPa)		Minimum Charpy Energy (J) at −20 °C	
	Nominal Thickness (mm)		Nominal Thickness (mm)		Transverse specimens	Longitudinal specimens
	≤ 16	>16 ≤ 40	<3	≥ 3 ≤ 100		
S275JR	275	265	430 to 580	410 to 560	–	27
S355J2	355	345	510 to 680	470 to 630	–	27
S460M	460	440	540 to 720	530 to 710	20	40
	≥ 3 ≤ 50	>50 ≤ 100	≥ 3 ≤ 50	>50 ≤ 100		
S690Q	690	650	770 to 940	760 to 930	30	30

a transition from brittle to ductile behavior with increasing temperature. The corresponding temperature range, where this transition occurs, is the so called ductile-to-brittle transition region (DBTR) [12].

The Master Curve (MC) approach, standardized in ASTM E1921 [11], offers a practical solution for characterizing the fracture behavior of ferritic steels in the DBTR [13,14]. The MC is based on the weakest link theory and, thus, describes the fracture behavior using a three parameter Weibull distribution, with the fundamental material parameter being the reference temperature (T_0). T_0 represents the temperature at which the median of fracture toughness, denoted as $K_{Jc,med}$, for a 1 T (25.4 mm) thick specimen equals 100 MPa$\sqrt{m}$. Once T_0 is defined for the material under consideration, the fracture toughness can be defined for any temperature (T) and probability of failure (P_f) through the MC equation:

$$K_{JC,\ Pf} = 20 + \left[ln\left(\frac{1}{1-P_f}\right)\right]^{1/4} \cdot \{11 + 77 \cdot exp[0.019 \cdot (T - T_0)]\} \quad (1)$$

Furthermore, when T_0 is determined by testing specimens with thicknesses different that 25.4 mm, as in the case of mini-C(T) specimens, the MC approach defined in ASTM E1921 [11] proposes a correction to transform the measured K_{Jc} values into their $K_{Jc,1T}$ equivalents, using equation (2), with B representing the thickness of the tested specimen:

$$K_{Jc,1T} = 20 + [K_{JC} - 20]\left(\frac{B}{25.4}\right)^{1/4} \quad (2)$$

The MC addresses the three main issues of fracture characterization within the DBTR: the scatter of the results, the temperature dependence of the fracture toughness, and the influence of the specimen thickness.

The first combination of the use of mini-C(T) specimens together with the MC approach was initially proposed by Scibetta in 2002 [15] and subsequently corroborated by Miura in 2010 [8]. Miura's work presented a T_0 in close agreement with those obtained using conventional fracture specimens. Since then, while the accuracy of the MC when derived from mini-C(T) specimens has been verified in a number of nuclear steel grades, under both irradiated and non-irradiated conditions (e.g., [7,9,10,16]), it is noteworthy that the validation on structural steels used in other sectors such as bridge construction, building, automotive or machinery, is either scarce or non-existent. Consequently, this work aims to contribute to the validation of mini-C(T) specimens as a tool to characterize the DBTR of common structural steels.

With this context in mind, the primary objectives of this paper are to contribute to the extensive validation of mini-C(T) specimens for determining the material MC, and to conduct a comparative analysis with results obtained from conventional (i.e., larger C(T) or SE (B) specimens, typically 25.4 mm-thick or 1 in.) fracture mechanics specimens. The study is specifically focused on four distinct structural steel grades (S275JR, S355J2, S460M and S690Q) that collectively encompass a wide spectrum of T_0 values. Section 2 of this paper sets out to describe the materials used, to outline the experimental program, and to explain the methodology applied to implement the MC approach using mini-C(T) specimens; Section 3 gathers and analyzes the experimental results, including the evaluation of T_0, along with a comprehensive examination of the underlying fracture micromechanisms, followed by the corresponding discussion and a comparison with numerous results from literature; Finally, in Section 4, the key conclusions of this study are summarized.

2. Materials and methods

2.1. Materials

The experimental program involved four distinct types of structural steels: S275JR, S355J2, S460M and S690Q (ASTM approximate equivalences: A36, A572 Gr. 50, A572 Gr. 65 and A514, respectively) [17,18]. S275JR and S355J2 steels were provided as 25 mm (1 T) thick, 1000 mm × 2500 mm rolled plates, while S460M and S690Q steels were supplied as 15 mm (0.6 T) thick, 1000 mm × 1500 mm rolled plates. The main supply conditions of this materials according to the European Standards are presented in Table 1. S275JR and S355J2 are non-alloy structural steels suitable for welding, with ferritic-pearlitic microstructures standardize in the UNE-EN 10025:2 [19]; S460M is a fine-grain, thermomechanically treated steel. The 'M' denotes that the steel has been thermomechanically rolled, as specified in UNE-EN 10025:4 [20]; finally, S690Q is a high-strength, quenched and tempered steel, where 'Q' stands for the quenched

Table 2
Chemical composition of the four structural steels (wt. %).

Material	C	Si	P	S	Cr	Mn	Ni	Cu	Mo	V	Nb	Al	Ti
S275JR	0.180	0.260	0.012	0.009	0.018	1.180	0.085	0.060	0.120	0.020	–	0.034	0.022
S355J2	0.200	0.320	0.012	0.008	0.050	1.390	0.090	0.060	0.120	0.020	–	0.014	0.022
S460M	0.120	0.450	0.012	0.001	0.062	1.490	0.016	0.011	–	0.066	0.036	0.048	0.003
S690Q	0.150	0.400	0.006	0.001	0.020	1.420	0.160	0.010	–	0.058	0.029	0.056	0.003

Table 3
Room temperature material properties along with T_0 derived from conventional (large) specimens. RT: room temperature; $\sigma_{y,RT}$: yield stress at RT; $\sigma_{u,RT}$: ultimate tensile strength at RT, $\varepsilon_{max,RT}$: uniform elongation at RT; T_0: reference temperature.

Material	Orientation	$\sigma_{y,RT}$ (MPa)	$\sigma_{u,RT}$ (MPa)	$\varepsilon_{max,RT}$ (%)	T_0 (°C)	Specimen type	Ref
S275JR	T-L	328.4	518.5	15.9	−26	1 T-C(T)	[25]
S355J2	T-L	376.4	557.6	15.4	−133	1 T-C(T)	[25]
S460M	T-L	473	595	30.0	−92	0.6 T-SE(B)	[18]
S690Q	T-L	775	832	20.0	−110	0.6 T-SE(B)	[18]

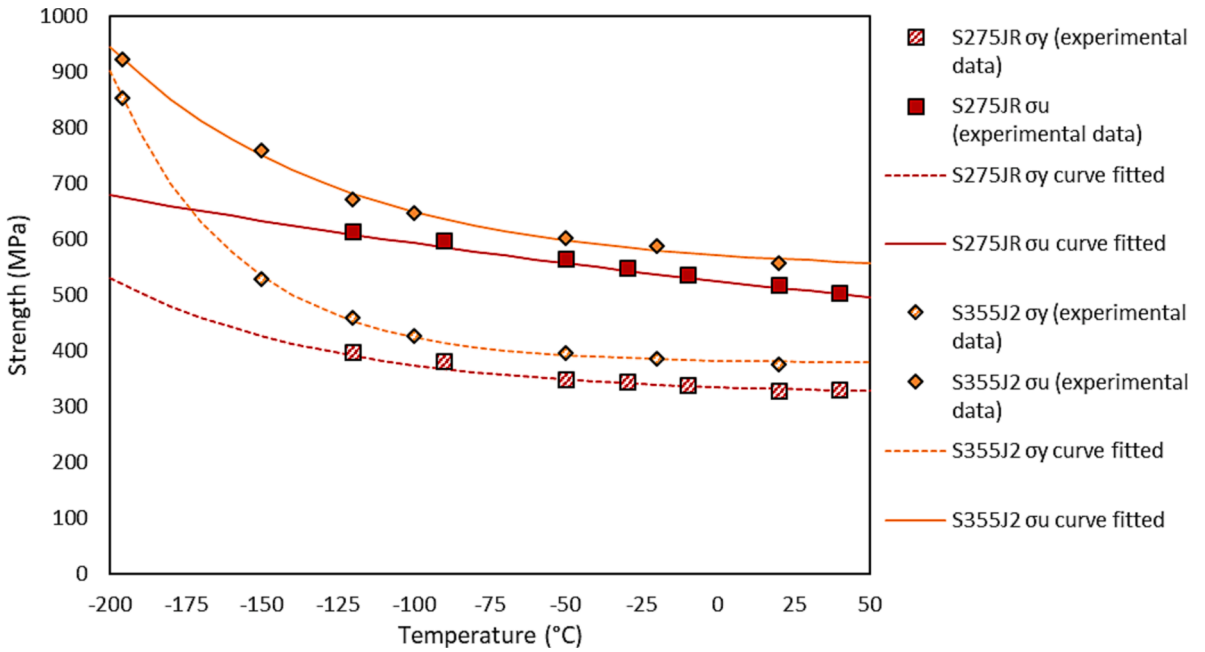

Fig. 1. Yield strength and ultimate tensile strength as a function of temperature for S275JR and S355J2 steels.

and tempered supply condition, with its microstructure being composed of bainite and tempered martensite, as specified by UNE-EN 10025:6 [21].

These four steels are commonly used in structural applications and exhibit a wide range of mechanical properties and chemical compositions, as summarized in Tables 2 and 3, respectively. Tensile tests were conducted following the ASTM E8/E8M [22], Charpy tests followed the ASTM E23 [23], and the fracture characterization within the ductile to brittle transition region was performed using conventional (i.e., 1 T-C(T) for S275JR and S355J2 and 0.6 T-SE(B) for S460M and S690Q) specimens following ASTM E1921-13 [24]. It is important to note that the MC characterization performed with conventional (1 T or 0.6 T) [18,25] specimens was carried out according to the 2013 version of the standard [24]. To ensure an unbiased comparison of the results between conventional specimens and mini-C(T) specimens, all the data obtained from conventional specimen testing were reprocessed using the 2021 version of the standard ASTM E1921 [11]. The appropriate master curve plots are presented below in the results section.

The tensile properties, such as the yield strength (σ_y) and the ultimate tensile strength (σ_u) of S275JR and S355J2 were determined across the ductile-to-brittle transition region of the materials, as shown in Fig. 1. However, in the case of S460M and S690Q steels, only room temperature (RT) properties were measured. For this reason, σ_y and the elastic modulus, E, were calculated for the selected test temperature based on equations (3) and (4) proposed by the ASTM E1921-21 [11].

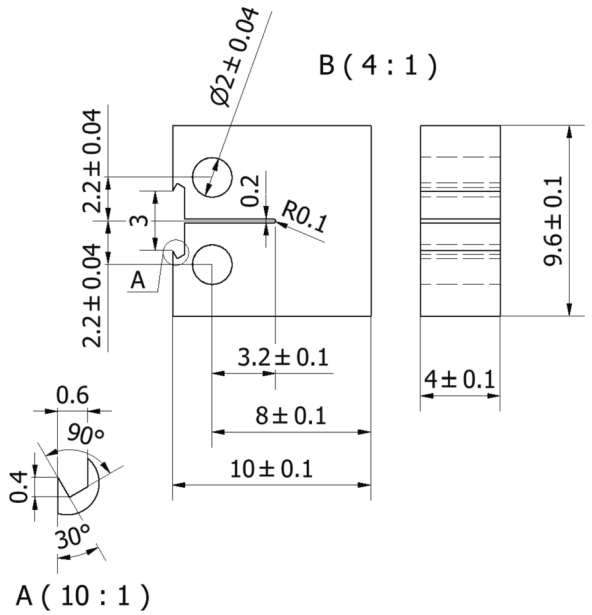

Fig. 2. The geometry of the mini-C(T) specimens. Dimensions in mm.

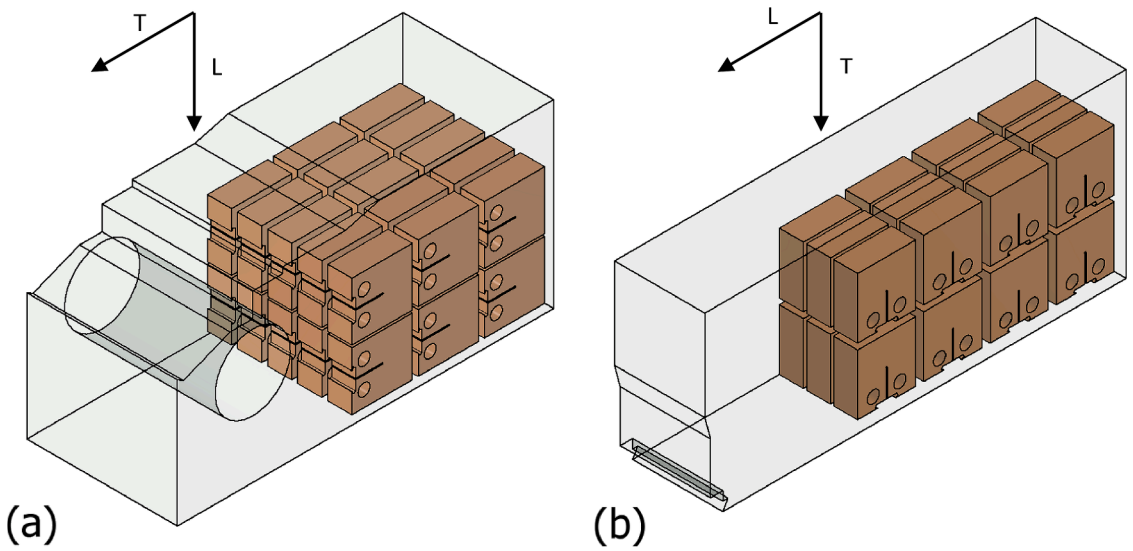

Fig. 3. Schematic of the mini-C(T) specimens extraction for (a) S275JR and S355J2 materials and (b) S460M and S690Q materials.

$$\sigma_y(\mathrm{MPa}) = \sigma_{yRT} + \frac{10^5}{(491 + 1.8T)} - 189 \tag{3}$$

$$E\,(\mathrm{GPa}) = 204 - \frac{T}{16} \tag{4}$$

2.2. Methods

2.2.1. Experimental program

The experimental campaign was conducted using 4 mm-thick C(T) specimens (B = 4 mm). This geometry is generally referred to as 0.16 T mini-C(T) specimens. The geometry selected, as shown in Fig. 2, is completely based on dimensional recommendations gathered in the ASTM E1921 [11], including a general tolerance of ± 0.013 W on all dimensions (approximately ± 0.1 mm), with W being the specimen width [11]. A total of 72 mini-C(T) specimens were extracted from the broken halves of the 1 T-C(T) and 0.6 T-SE(B) tested

Fig. 4. Experimental setup for testing mini-C(T) specimens.

specimens mentioned above [17,18], keeping the same orientation (LT) and also making sure that the material used had not developed plastic damage during the original tests, as can be observed from the location of the mini-C(T) specimens shown in Fig. 3.

In order to mount the clip-gage for measuring crack mouth opening displacement (CMOD), knife-edges were machined on the front face (see Fig. 2). CMOD was then converted to the load-line displacement by applying a rotational factor equation derived by Landes [26]:

$$R = \frac{v_{LL}}{v_{FF}} = \frac{a/W + r \cdot (1 - a/W)}{a/W + r \cdot (1 - a/W) + X/W} \tag{5}$$

where r is the ratio of the distance from the crack tip to the point of rotation divided by the remnant ligament (b_0), and X is the offset between the front face and the load line (i.e., the line defined by the points where the loads are applied to the specimen). Landes recommended r = 0.33: thus, the conversion factor for a standard C(T) specimen with a/W = 0.5 and X/W = 0.25 was 0.73, which is the actual value recommended by the ASTM E1921 [11]. These load-line displacements were used to determine the J integral value at cleavage onset, since its plastic part, J_p, is defined based on the corresponding load-line displacement. It is important to note that, in this study, the side grooving technique was not considered given its demonstrated minimal impact on this type of small specimens [27], which in addition would reduce the measuring capacity, and would increase the machining costs, among other factors.

The testing procedure and the subsequent analysis were performed following the ASTM E1921-21 standard [11]. Before conducting the tests, crack-like defects were introduced by fatigue pre-cracking. The length of the resulting cracks was controlled by optical microscopy techniques together with CMOD measurements through compliance measurements, ensuring a final pre-crack length within the range of 0.5 W ± 0.05 W (3.6 to 4.4 mm), as specified in ASTM E1921 [11].

The specimens were cooled to the selected temperature in a thermostatic chamber fed by liquid nitrogen, with electronic control in the range of ± 1 °C by means of a thermocouple. To ensure a homogeneous temperature throughout the entire specimen during the test, specimens were maintained at the temperature for at least 15 min before starting the fracture test. While ASTM E1921 [11] recommends attaching a thermocouple directly to the specimen, scientific literature accepts the temperature being monitored by a thermocouple attached to the surface of the clevis, assuming differences in the range of ± 3 °C between the clevis and specimen [9]. In the present work, for the sake of operational simplicity and to avoid any possible effects of heat input, this latter option was chosen. The initial test temperature for each material was selected by lowering the T_0 values obtained by conventional specimens (shown in Table 2) by about 30 °C-35 °C, as recommended in [8] with the aim of reducing the possibility of data censoring derived from the $K_{Jc,limit}$ criterion (see section 2.2.3 for further information).

The tests were conducted using a servo hydraulic machine, at a quasi-static loading rate of 1 MPa$\sqrt{m}$/s, inside the range between 0.1 MPa$\sqrt{m}$/s to 2 MPa$\sqrt{m}$/s recommended by ASTM E1921 [11]. During the tests, both the force and the front face displacement

Table 4
Master curve analysis input for S275JR.

Code	Temperature (°C)	$K_{Jc,0.16T}$ (MPa$\sqrt{m}$)	$K_{Jc,limit\ 0.16T}$ (MPa$\sqrt{m}$)	a_0 (mm)	Δa_p (mm)	δ_i	$K_{Jc,1T}$ (MPa$\sqrt{m}$)
S275_01	**−50**	**354.04**	**100.12**	**4.27**	**1.17**	**0**	**70.28**
S275_02	**−65**	**237.40**	**100.20**	**4.33**	**0.18**	**0**	**70.52**
S275_03	**−75**	**214.53**	**100.13**	**4.40**	**0.14**	**0**	**70.48**
S275_04	**−90**	**255.55**	**101.69**	**4.40**	**0.55**	**0**	**71.46**
S275_05	−110	86.68	106.81	4.33	0.00	1	62.01
S275_06	−110	75.72	107.90	4.25	0.00	1	55.10
S275_07[1]	−120	38.61	103.89	4.42	0.00	1	31.72
S275_09	−100	59.39	104.84	4.26	0.00	1	44.81
S275_10	**−80**	**240.28**	**103.29**	**4.21**	**0.00**	**0**	**72.47**
S275_11	**−90**	**186.74**	**103.93**	**4.24**	**0.00**	**0**	**72.87**
S275_12	**−100**	**154.61**	**103.45**	**4.36**	**0.00**	**0**	**72.57**
S275_13	−100	103.09	103.12	4.38	0.00	1	72.35
S275_15	**−100**	**166.73**	**102.88**	**4.40**	**0.00**	**0**	**72.21**
S275_16	−105	66.82	105.56	4.26	0.00	1	49.49
S275_17	−105	79.48	105.09	4.29	0.00	1	57.47
S275_18	−105	69.52	105.99	4.23	0.00	1	51.19
S275_19	−105	57.84	103.54	4.40	0.00	1	43.84

[1] Outside the temperature validity range $-50\ °C < T\text{-}T_0 < 50\ °C$.

Table 5
Master curve analysis input for S355J2.

Code	Temperature (°C)	$K_{Jc,0.16T}$ (MPa$\sqrt{m}$)	$K_{Jc,limit}$ (MPa$\sqrt{m}$)	a_0 (mm)	Δa_p (mm)	δ_i	$K_{Jc,1T}$ (MPa$\sqrt{m}$)
S355_02	−145	68.28	122.00	4.31	0.00	1	50.41
S355_03	−155	66.64	127.11	4.27	0.00	1	49.27
S355_05	**−120**	**154.93**	**112.85**	**4.38**	**0.00**	**0**	**78.49**
S355_06	**−130**	**160.97**	**115.19**	**4.40**	**0.00**	**0**	**79.96**
S355_07[1]	−145	75.84	118.22	4.53	0.00	1	55.18
S355_08	−145	56.50	124.30	4.17	0.00	1	42.99
S355_09	**−135**	**156.08**	**118.93**	**4.26**	**0.00**	**0**	**82.32**
S355_10	−145	98.43	121.62	4.33	0.00	1	69.41
S355_11	−145	117.12	126.54	4.03	0.00	1	81.18
S355_13	−145	107.36	120.44	4.40	0.00	1	75.03
S355_14[2]	−165	81.44	136.57	4.05	0.00	1	58.70
S355_15	−145	64.00	120.87	4.37	0.00	1	47.72
S355_16	−140	70.81	118.50	4.40	0.00	1	52.01
S355_17	−140	108.37	118.73	4.39	0.00	1	75.67
S355_18	−140	81.05	120.58	4.27	0.00	1	58.46
S355_19	−155	83.89	129.14	4.16	0.00	1	60.25
S355_20	−140	74.91	120.67	4.27	0.00	1	54.59
S355_21[1]	−140	81.16	115.89	4.56	0.00	1	58.53
S355_22	−135	78.69	117.02	4.38	0.00	1	56.97

[1] Discarded because of $a_0/W > 0.55$.
[2] Outside the temperature validity range $-50\ °C < T\text{-}T_0 < 50\ °C$.

(measured using a clip-gage) were continuously recorded. The experimental setup is illustrated in Fig. 4.

From the broken halves of each specimen, the real initial crack length was determined by averaging the nine measurements as specified the ASTM E1921 [11]. This evaluated crack length was subsequently employed for further calculations. In addition, crack straightness for every specimen was checked in accordance with the criterion of ASTM E1921 [11].

2.2.2. Master curve evaluation

The assessment of fracture toughness within the DBTR test involved determining K_{Jc} for mini-C(T) specimens. This elastic–plastic parameter, expressed in terms of stress intensity factor, is derived from the J integral at the onset of cleavage fracture (J_c). The relationship between these two parameters is given by equation (6):

$$K_{Jc} = \sqrt{J_c \bullet \frac{E}{(1-\nu^2)}} \tag{6}$$

Here, E represents the Young's modulus, and ν is the Poisson's ratio. The K_{Jc} values used to define the MC are considered valid under specific criteria, including high constraint, small-scale yielding, and microstructural evidence of cleavage fracture. Notably, the maximum K_{Jc} capacity that guarantees high constraint conditions depends on the remaining ligament (b_0) of the specimen (which is

Table 6
Master curve analysis input for S460M.

Code	Temperature (°C)	$K_{Jc,0.16T}$ (MPa·√m)	$K_{Jc,limit}$ (MPa·√m)	a_0 (mm)	Δa_p (mm)	δ_i	$K_{Jc,1T}$ (MPa·√m)
S460_01[1]	**−100**	**269.00**	**128.40**	**4.54**	**0.76**	**0**	**84.36**
S460_02	**−120**	**151.15**	**139.23**	**4.19**	**0.00**	**0**	**94.48**
S460_03[1]	**−130**	**224.71**	**135.98**	**4.55**	**0.00**	**0**	**92.06**
S460_04[1]	**−135**	**186.94**	**137.45**	**4.53**	**0.00**	**0**	**93.22**
S460_05	−145	99.31	140.76	4.40	0.00	1	69.96
S460_06	−145	45.81	144.02	4.31	0.00	1	36.26
S460_08[1]	**−140**	**166.36**	**139.42**	**4.54**	**0.00**	**0**	**94.08**
S460_09	**−145**	**171.00**	**145.96**	**4.31**	**0.00**	**0**	**97.99**
S460_10[1]	−150	100.88	147.75	4.51	0.00	1	70.95
S460_11[1]	−150	122.17	137.11	4.78	0.00	1	84.36
S460_12[1]	−155	95.21	139.50	4.71	0.00	1	67.38
S460_13[1]	−155	92.38	143.07	4.54	0.00	1	65.60
S460_14[1]	−155	47.10	143.63	4.51	0.00	1	37.07
S460_15[1]	−150	81.42	139.18	4.63	0.00	1	58.69
S460_16	−150	70.06	143.13	4.44	0.00	1	51.54
S460_17	−150	91.27	145.89	4.30	0.00	1	64.90
S460_18[1]	−150	76.56	139.95	4.60	0.00	1	55.63
S460_19[1]	−150	103.38	141.16	4.54	0.00	1	72.52
S460_20[1]	−150	104.00	137.78	4.70	0.00	1	72.92

[1] Discarded because of $a_0/W > 0.55$.

Table 7
Master curve analysis input for S690Q.

Code	Temperature (°C)	$K_{Jc,0.16T}$ (MPa·√m)	$K_{Jc,limit}$ (MPa·√m)	a_0 (mm)	DCG (mm)	δ_i	$K_{Jc,1T}$ (MPa·√m)
S690_01[1]	−140	57.77	165.28	4.51	0.00	1	43.80
S690_03	−130	77.56	164.24	4.44	0.00	1	56.26
S690_04	−130	84.42	166.37	4.35	0.00	1	60.58
S690_05	−120	61.35	162.79	4.40	0.00	1	46.05
S690_06	−110	76.27	161.46	4.40	0.00	1	55.45
S690_07[1]	**−90**	**205.88**	**147.81**	**4.80**	**0.00**	**0**	**100.52**
S690_08	**−100**	**160.88**	**158.72**	**4.40**	**0.00**	**0**	**107.39**
S690_09[1]	−100	114.93	154.61	4.58	0.00	1	79.80
S690_10[1]	**−100**	**169.64**	**153.97**	**4.61**	**0.00**	**0**	**104.39**
S690_11	−100	126.22	158.63	4.40	0.00	1	86.91
S690_12	−100	127.70	157.58	4.45	0.00	1	87.85
S690_13	**−100**	**150.34**	**158.64**	**4.40**	**0.26**	**0**	**102.11**
S690_14	−105	118.21	159.61	4.40	0.00	1	81.87
S690_15[1]	−105	80.16	153.41	4.67	0.00	1	57.90
S690_16[1]	−105	139.84	153.32	4.68	0.00	1	95.50
S690_17[1]	−105	93.42	150.63	4.79	0.00	1	66.25
S690_18	−105	140.43	163.14	4.24	0.00	1	95.87

[1] Discarded because of $a_0/W > 0.55$.

defined as the difference between the width, W, and the initial crack length, a_0), as indicated in equation (7). K_{Jc} data exceeding this limit must be replaced (censored) by the corresponding $K_{Jc,limit}$ value.

$$K_{Jc,limit} = \sqrt{\frac{E \bullet b_0 \bullet \sigma_y}{30 \bullet (1-\nu^2)}} \tag{7}$$

Equation (7) is particularly important when using mini-C(T) specimens, as their small dimensions (i.e., small b_0 values) increase the likelihood of censoring K_{Jc} data obtained at temperatures near or above T_0. Furthermore, ductile crack growth is restricted to values below 0.05(W-a_0), which corresponds to about 0.2 mm for mini-C(T) specimens, or 1 mm, whichever is smaller. If this criterion is not met, the corresponding K_{Jc} value is censored, and the highest uncensored K_{Jc} value in the entire dataset is used instead. After applying the two-step censoring procedure (as described in section 8.9.2 of ASTM E1921 [11]), the subsequent step involves converting K_{Jc} values obtained from 4 mm-thick specimens (mini-C(T)s) into $K_{Jc,1T}$ (equivalent to 1 T or 25.4 mm) values using equation (2).

In this study, T_0 is determined from the resulting $K_{Jc,1T}$ dataset using the multi-temperature method, following ASTM E1921 [11]. An initial estimate of T_0, denoted as T_{0Q}, is obtained from equation (8):

$$\sum_{i=1}^{N} \delta_i \bullet \frac{\exp[0.019 \bullet (T_i - T_{0Q})]}{11 + 77 \bullet \exp[0.019 \bullet (T_i - T_{0Q})]} - \sum_{i=1}^{N} \frac{(K_{Jc,i,} - 20)\exp[0.019 \bullet (T_i - T_{0Q})]}{\{11 + 77 \bullet \exp[0.019 \bullet (T_i - T_{0Q})]\}^5} = 0 \tag{8}$$

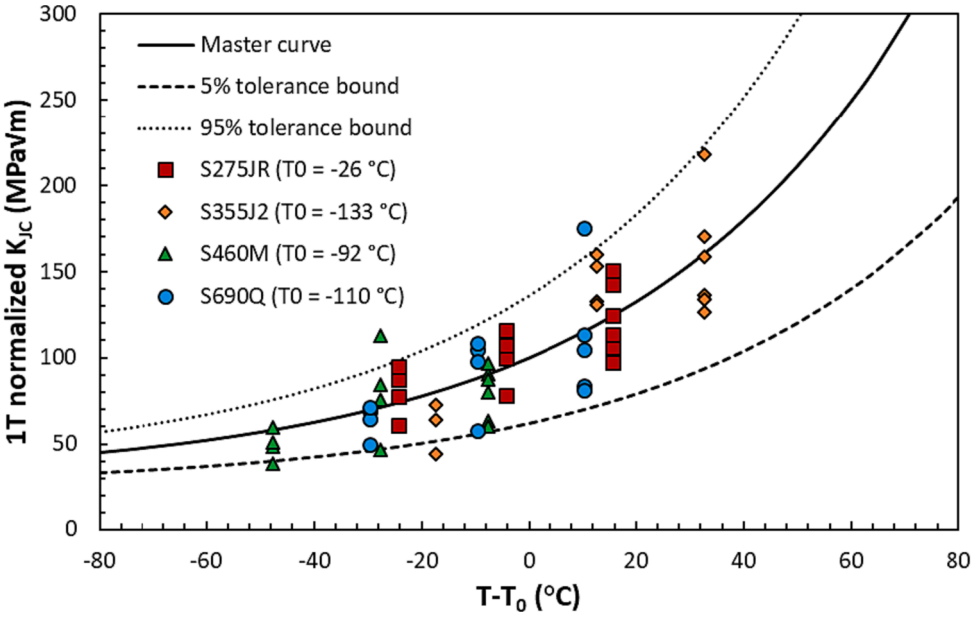

Fig. 5. Master-Curve analysis using 1 T-C(T) and 0.6 T-SE(B) specimens [18,25].

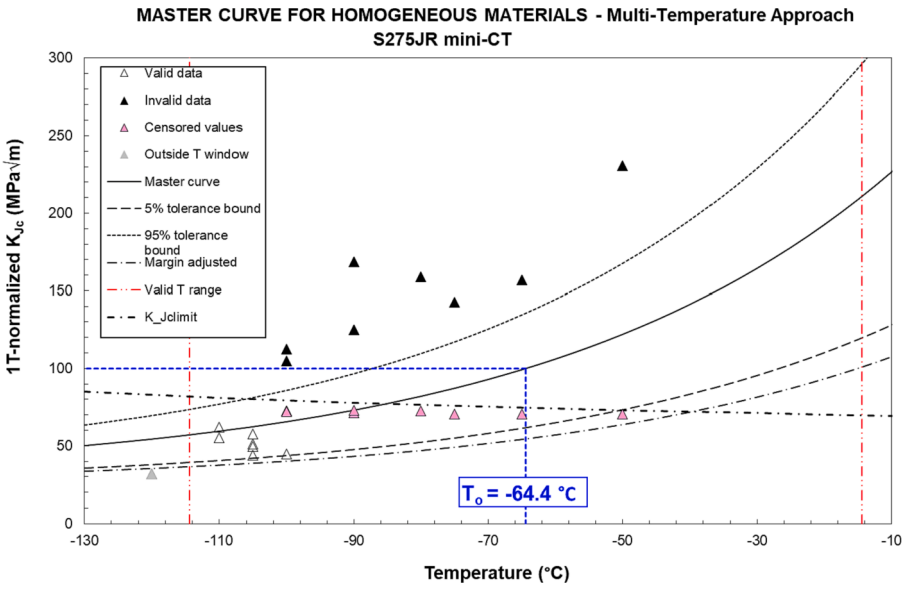

Fig. 6. Mini-C(T) based Master-Curve analysis for S275JR.

Here, N represents the number of tested specimens, T_i is the test temperature corresponding to the $K_{Jc,i}$ value, and T_{0Q} is a provisional value of T_0. T_{0Q} is later qualified as T_0 if two additional conditions are met: the data used in the calculations fall within the temperature range of $T_0 \pm 50$ °C, and condition (9) is satisfied:

$$\sum_{i=1}^{n} r_i \bullet n_i \geq 1 \tag{9}$$

where r_i denotes the number of uncensored data, and n_i represents the specimen weighting factor (as per Table 5 in section 10.3 of ASTM E1921 [11]). Once T_0 is determined, the relation between $K_{Jc,med}$ and T is described by equation (9):

$$K_{Jc,med} = 30 + 70 \bullet \exp[0.019 \bullet (T - T_0)] \tag{10}$$

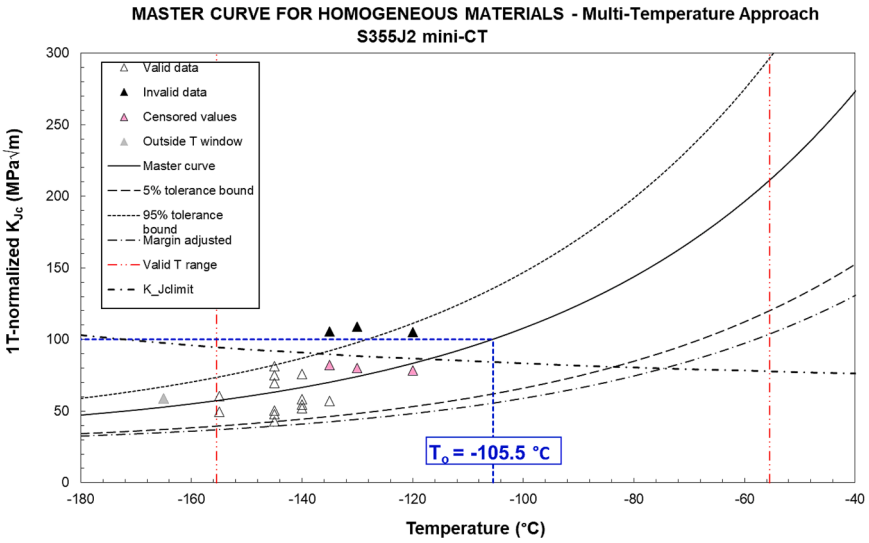

Fig. 7. Mini-C(T) based Master-Curve analysis for S355J2.

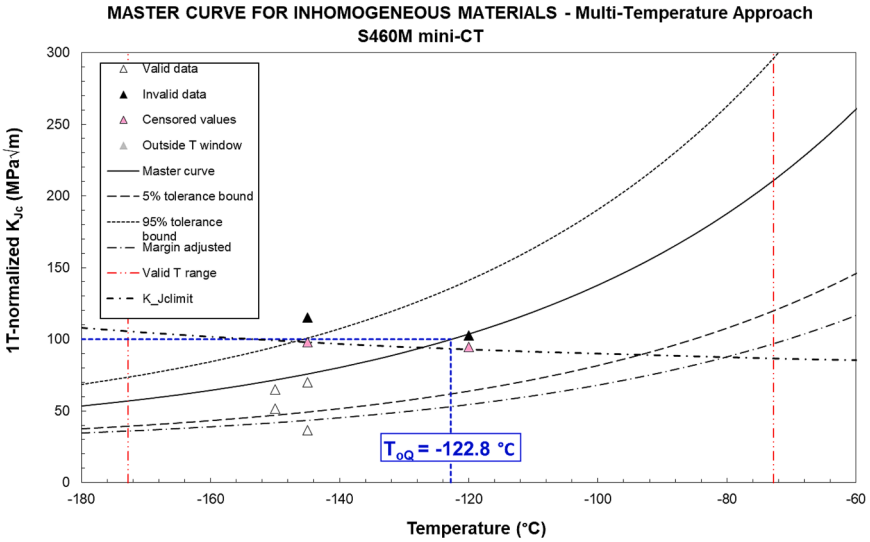

Fig. 8. Mini-C(T) based Master-Curve analysis for S460M.

Additionally, the K_{Jc} value for any probability of failure (P_f) and working temperature (T) can be calculated using equation (1), with the most common curves associated with probabilities of failure of 5 % and 95 % being provided by equations (11) and (12), respectively:

$$K_{Jc,0.05} = 25.2 + 36.6 \bullet \exp[0.019 \bullet (T - T_0)] \tag{11}$$

$$K_{Jc,0.95} = 34.5 + 101.3 \bullet \exp[0.019 \bullet (T - T_0)] \tag{12}$$

Finally, the standard deviation (σ_{T0}) of T_0 is calculated as:

$$\sigma_{T0} = \left(\frac{\beta^2}{r} + \sigma_{exp}^2\right)^{1/2} \tag{13}$$

where β is the sample size uncertainty factor determined following section 10.9.1 in ASTM E1921 [11], r represents the total number of uncensored data used to calculate T_0 and σ_{exp} denotes the contribution of experimental uncertainties, typically assumed to be 4 °C.

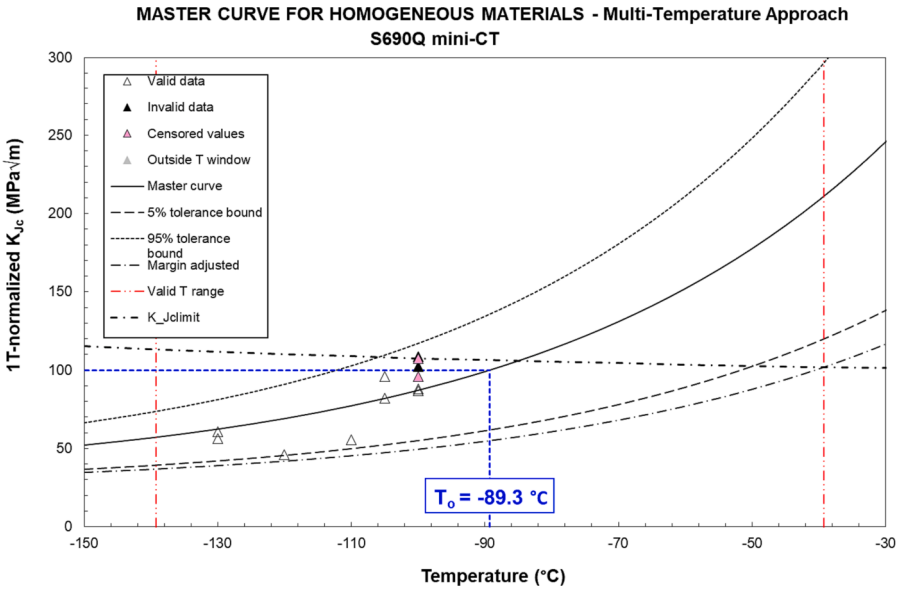

Fig. 9. Mini-C(T) based Master-Curve analysis for S690Q.

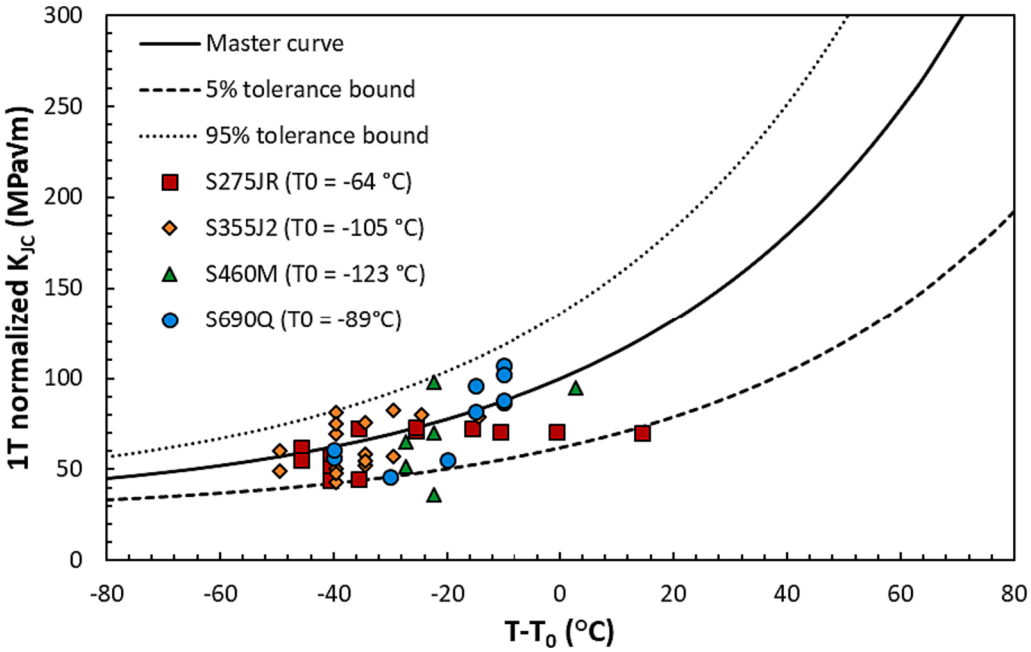

Fig. 10. Master Curve analyses using mini-C(T) specimens.

3. Results and discussion

3.1. Reference temperature evaluation

Tables 4 to 7 present all the data obtained from the conducted tests, which serves as the input for the MC evaluation. The information includes the testing temperature, the experimental fracture toughness value for each individual test obtained from 0.16 T mini-C(T) specimens ($K_{Jc,0.16T}$), the corresponding $K_{Jc,limit}$ values ($K_{Jc,limit\ 0.16T}$), the initial crack size measured on the broken specimens, the amount of ductile crack growth (Δa_p, if any), the censoring condition (δ_i) and the resulting $K_{Jc,1T}$ values to be used in the estimation of T_0. Here, it is important to note that censored $K_{Jc,1T}$ values ($\delta_i = 0$) are represented in the tables by the corresponding censored value (in bold characters), and not by the direct conversion of $K_{Jc,0.16\ T}$ into the 1 T equivalent using equation (2), as in the case of non-

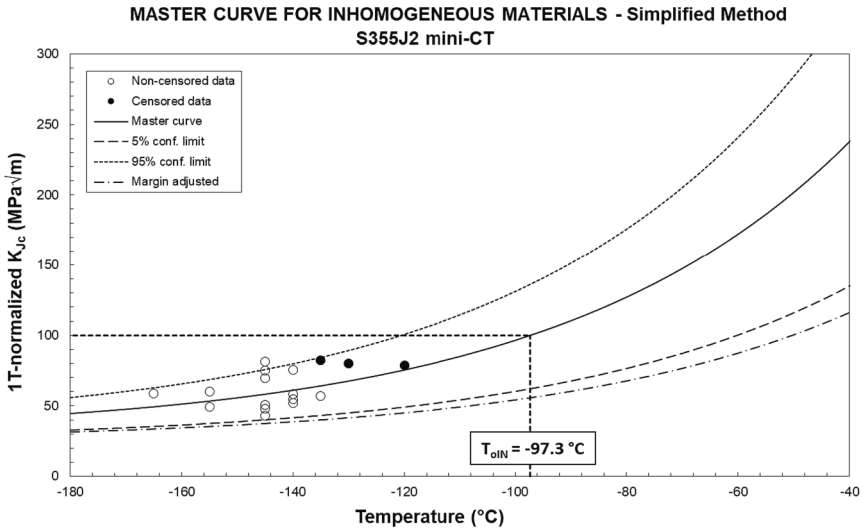

Fig. 11. Mini-C(T) based Master Curve Simplified Method analysis for S355J2.

Table 8
Summary of the MC analysis performed in the structural steels.

Material	Dataset	T_0 (°C)	σ_{T0} (°C)	$T_{0,\ scrn}$ (°C)	r	N	$\sum r_i \bullet n_i$	Homogeneity screening
S275JR	1 T-C(T)	−26	6.26	−30	14	14	2.24	Homogeneous
	Mini-C(T)	−64	8.15	−64	8	16	1.00	Homogeneous
S355J2	1 T-C(T)	−133	6.40	−129	13	13	2.10	Homogeneous
	Mini-C(T)	−105	6.86	−97	13	16	1.46	Inhomogeneous
S460M	0.6 T-SE(B)	−92	6.26	−87	14	14	2.07	Homogeneous
	Mini-C(T)	−123*	10.22	−110	4	6	0.57	Homogeneous
S690Q	0.6 T-SE(B)	−110	6.40	−106	13	13	2.07	Homogeneous
	Mini-C(T)	−89	7.76	−87	8	10	1.15	Homogeneous

*T_{0Q} according to ASTM E1921 [11].

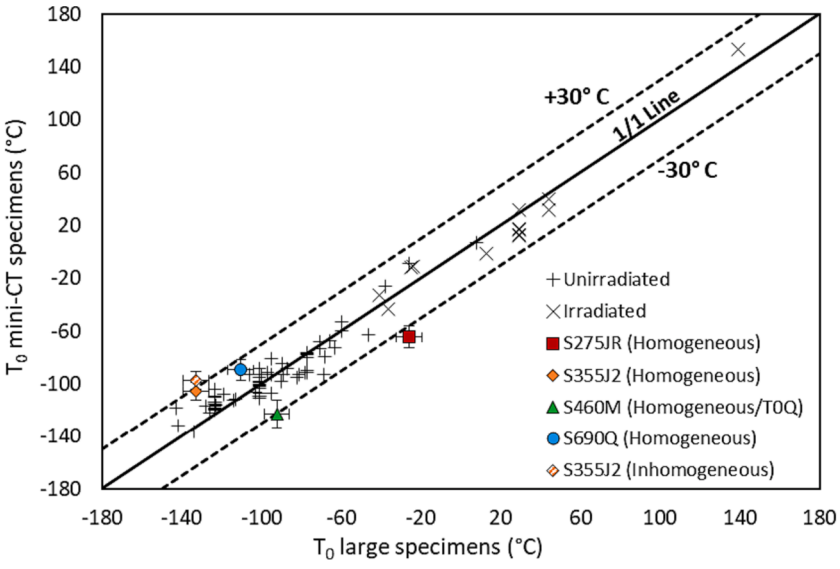

Fig. 12. Comparison between T_0 values from conventional specimens and T_0 values obtained using mini-C(T) specimens [28].

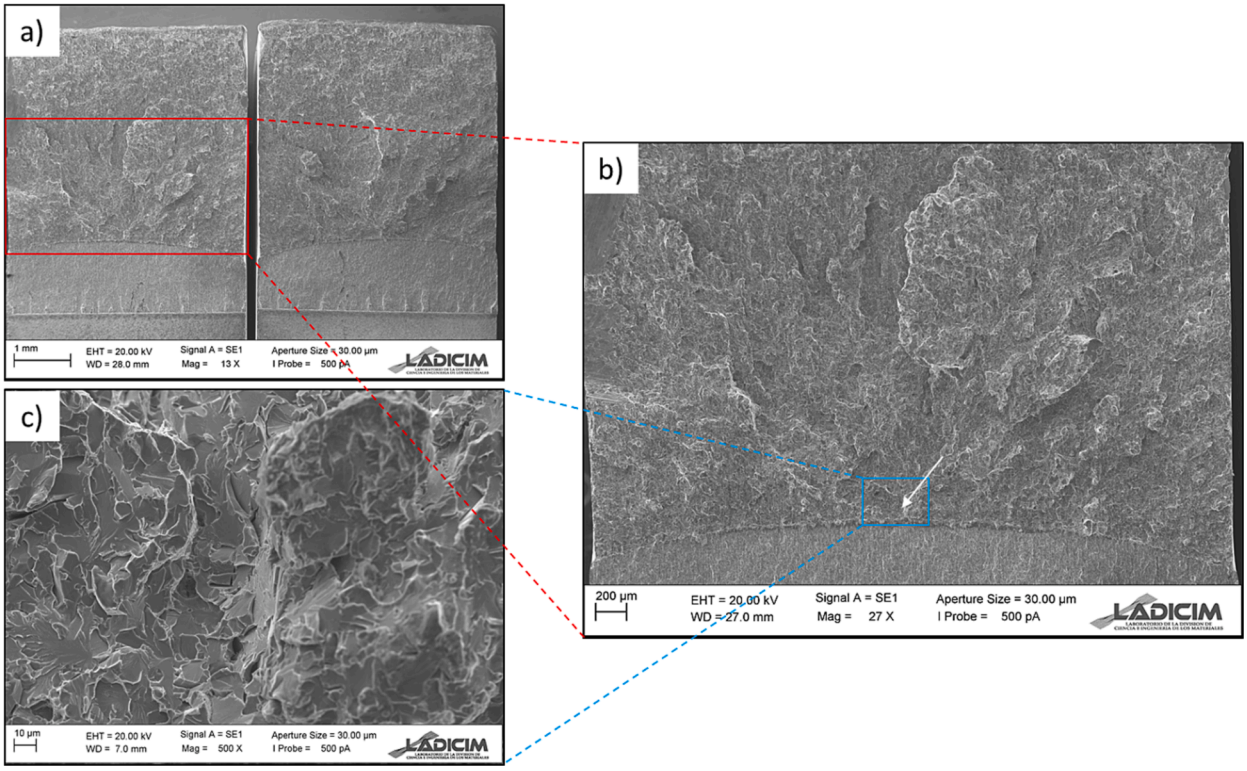

Fig. 13. SEM analysis of S275JR_13 specimen (T = -100 °C / $K_{Jc,0.16T}$ = 103 MPa$\sqrt{m}$): a) overview of the two halves; b) crack front and fracture surface; c) detail of the initiation area.

censored values ($\delta_i = 1$). Additionally certain results were excluded based on the crack length criterion of $a_0/W = 0.5 \pm 0.05$, in accordance with ASTM E1921 [11]. As a result, 51 out of 72 specimens were ultimately utilized for the MC analysis. The number of acceptable tests was 17, 17, 6 and 10 for S275JR, S355J2, S460M and S690Q, respectively. It is worth noting that all the crack fronts satisfied the straightness criterion established in section 8.9.1 of ASTM E1921 [11].

For the S275JR material (see Table 4), 8 K_{Jc} values were censored ($\delta_i = 0$) since they exceeded one of two censoring criteria: excessive ductile crack growth (greater than 0.02 mm) or K_{Jc} greater than $K_{Jc,limit}$, or both. In all these cases, the values were eventually censored by $K_{Jc,limit}$, which was the most limiting condition following the ASTM E1921 [11]. Therefore, these K_{Jc} values were replaced by the corresponding 1 T-scaled $K_{Jc,limit}$ value. Additionally, one value did not meet the temperature range criteria, resulting in a MC analysis based on 16 specimens. The results show that the final T_0 is derived from a significant number of censored values but, this being said, the obtained T_0 is valid according to the standard (equation (9)).

In the case of steel S355J2 (see Table 5), three specimens exceeding $K_{Jc,limit}$ were censored. Consequently, these values were replaced by the corresponding 1 T-scaled $K_{Jc,limit}$. Moreover, one test was performed outside the temperature validity range, so the corresponding result was discarded. Therefore, the final dataset utilized for the MC consisted of 16 specimens.

The S460M steel (detailed in Table 6) presented a particular scenario in which most of the specimens did not meet the initial crack length to width ratio criteria, with the majority falling between $0.56 < a_0/W < 0.6$. Therefore, the MC analysis was based on only six valid specimens, two of which were censored by the $K_{Jc,limit}$ criterion.

In the case of the S690Q grade (see Table 7), one value was censored by the $K_{Jc,limit}$ criterion, and another value was censored by the Δa_p criterion (it exceeded 0.2 mm). Therefore, in the latter case, the K_{Jc} value was replaced with the maximum non-censored value within the dataset.

Fig. 5 summarizes the original characterization of the four structural steels, performed on conventional specimens: 1 T-C(T) specimens (steels S275JR and S355J2) and 0.6 T-SE(B) specimens (S460M and S690Q steels). It can be observed how the MC provides a good fitting of the experimental results obtained within the corresponding DBTR. The figure includes the 5 % and 95 % tolerance bounds (equations (10) and (11)) and the validity zone of the MC ($T_0 \pm 50$ °C and $K_{Jc,limit}$). It is worth noting that, as previously mentioned, all the historical data have been re-analyzed following the ASTM E1921-21 version of the standard [11], but negligible differences were found in the T_0 estimated values when compared to the original analysis (results shown in Table 2).

Figs. 6 to 9 show the results obtained for each steel when using mini-C(T) specimens, with Fig. 10 providing an overall view of all the results. Overall, for all the four steels under analysis, the MC provides a good fit of the experimental results obtained from mini-C(T) specimens. It can be observed in Fig. 10 that most of the K_{Jc} values lie within the 5 and 95 % confidence bands (46 out of 48). In the case of conventional specimens (see Fig. 5), a total of 48 out of 54 experimental results fall within the confidence bands. Therefore, it can be

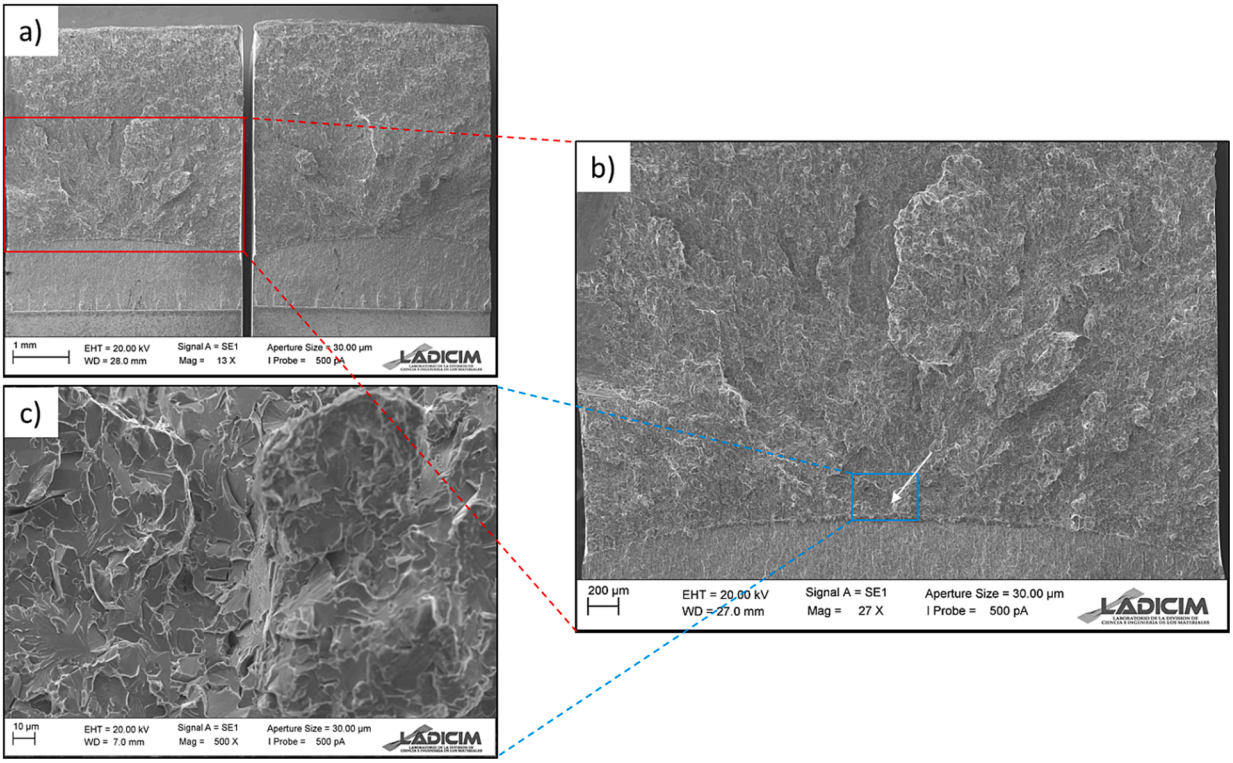

Fig. 14. SEM analysis of S355J2_22 specimen (T = -135 °C / $K_{Jc,0.16T}$ = 78 MPa$\sqrt{m}$): a) overview of the two halves; b) crack front and fracture surface; c) detail of the initiation area.

concluded that the capacity of the MC to estimate K_{Jc} values with mini-C(T) specimens is (at least) as good as that achieved with conventional specimens.

Furthermore, it can be observed that the validity zone (area below the censoring line and within $T_0 \pm 50$ °C) for mini-C(T) results is quite narrow. Since the remaining ligament is related to the specimen's thickness, reducing the thickness results in lower values of $K_{Jc,limit}$. This makes it advisable to conduct tests well below T_0 (e.g., $T_0 - 30$ °C) to obtain enough uncensored values, while still ensuring that the temperature range required for T_0 analysis is not violated. In other words, the practical testing temperature window when using mini-C(T) specimens is approximately $-50\ °C \leq T\text{-}T_0 \leq -30\ °C$.

With all the above considerations, valid T_0 values for mini-C(T) were determined as follows: $-64\ °C \pm 6.3\ °C$ for S275JR, $-105\ °C \pm 6.9\ °C$ for S355J2, and $-89\ °C \pm 7.8\ °C$ for S690Q. In the case of S460M, due to the high number of discarded data, a T_{0Q} value (i.e., not qualified as T_0) of $-123\ °C \pm 10.2\ °C$ was determined. In comparison with the T_0 values obtained from large specimens (shown in Table 2 and corresponding to −26 °C, −133 °C, −92 °C and −110 °C for S275JR, S355J2, S460M and S690Q, respectively), S275JR exhibits the largest difference ($T_{0mini\text{-}C(T)} - T_{0conventional}$), −38 °C. This is followed by S460M with a difference of −30.4 °C, S355J2 with a difference of +27.5 °C and finally S690Q with a difference of +21.1 °C.

Moreover, the homogeneity of the materials was assessed using the screening procedure provided by Section 10.6.2 of ASTM E1921 [11], which is based on a lower tail maximum likelihood estimation and performs an iterative process in the determination of the screening reference temperature (T_{0scrn}). According to this analysis, the S355J2 material was identified as inhomogeneous because it did not meet the screening criterion shown in equation (14) below. However, it is important to note that it exceeded the screening criterion by only a few tenths of a degree Celsius. The remaining structural steels met the screening criterion and were thus qualified as homogeneous. For S355J2, Appendix X.5, Section X.5.2 (Simplified Method) was applied to obtain a conservative estimate of the reference temperature for inhomogeneous materials (T_{0IN}), which was −97 °C, as shown in Fig. 11. In this particular case, T_{0IN} coincided with T_{0scrn}, as defined by [11]. This corresponds to a difference of + 36 °C when compared to the reference temperature obtained with 1 T-C(T) specimens, whose original analysis did not detect any inhomogeneity.

$$T_{0scrn} - T_0 \leq 1.44\sqrt{\frac{\beta^2}{r}} \tag{14}$$

A summary of all these results is presented in Table 8. Here, it is worth mentioning that, in addition to the analyses performed above, the difference in specimen geometry (C(T) vs SE(B)) may be playing a role. There is a well-known bias in T_0 of about 10 °C-15 °C between the two geometries, being C(T) the one expected to generate higher T_0 values [11].Thus, and considering the uncertainty of

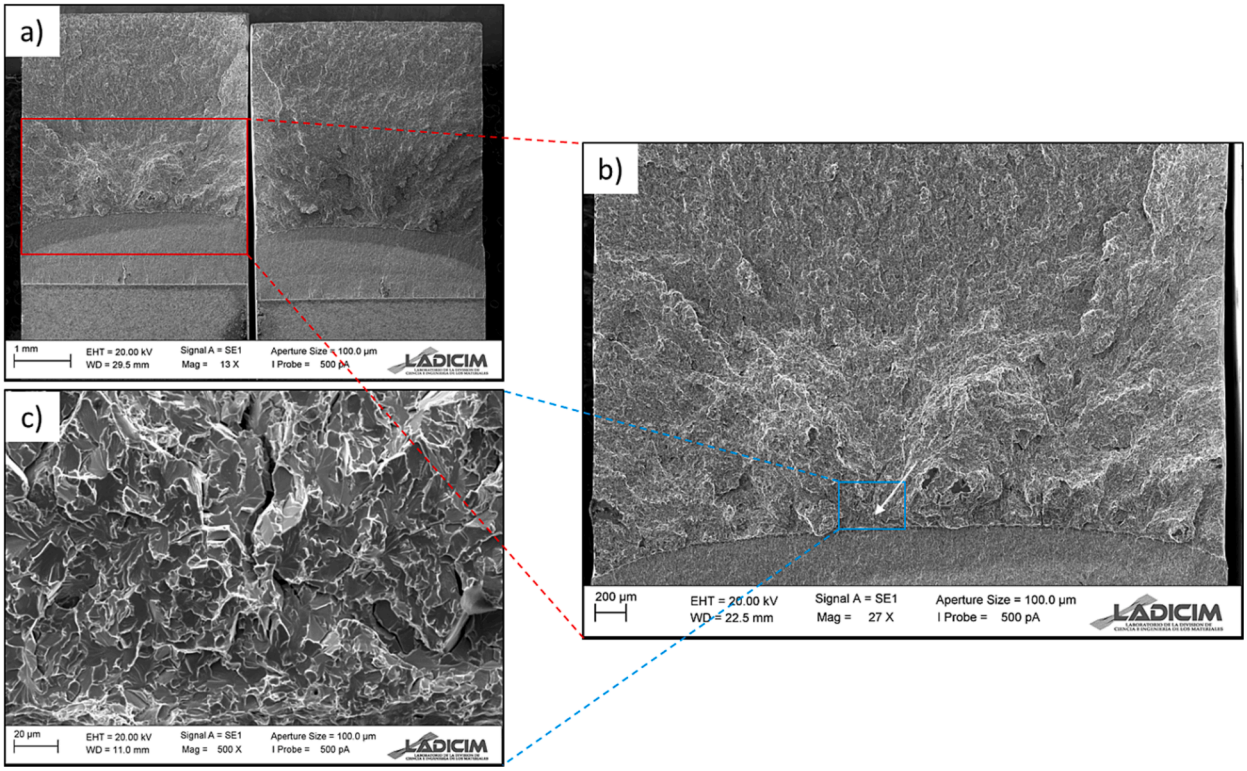

Fig. 15. SEM analysis of S460M_05 specimen (T = -145 °C / $K_{Jc,0.16T}$ = 99 MPa$\sqrt{m}$: a) overview of the two halves; b) crack front and fracture surface; c) detail of the initiation area.

the results, the results on steel S690Q are quite accurate. However, the results in steel S460M are less precise, something that may be related with the fact that the number of valid tests is reduced and the final reference temperature is not qualified as T_0.

For a better assessment of the capability of mini-C(T) specimens to determine T_0 and, consequently, the corresponding MC, a comparison was made between T_0 predictions obtained for structural steels and for nuclear steel grades. This analysis was based on a prior literature review conducted by the authors [28], which included results in base metals and weld metals of nuclear steels in both unirradiated and irradiated conditions. In these materials T_0 was obtained by using C(T) and SE(B) specimens with thicknesses ranging from 0.5 T to 2 T (i.e., 12.7 mm to 50.8 mm), and using mini-C(T) specimens. As observed in Fig. 12, all the nuclear grades fall within a range of ± 30 °C, and the results obtained here on structural steels are close to these limits. The results obtained in this work generally meet the +- 30 °C criterion, very in the limit, and tend to be within the largest variations found in literature. The reasons why the results in these structural steels are these may be diverse, and include the fact that one of the points (steel S460M) represents a T_{0Q} value, and other material (S355J2) is identified as inhomogeneous in the MC analysis. Further research is needed to delve deeper into this issue Notably, published data (including the results presented in this paper) exhibit an interesting behavior: in some cases, mini-C(T) specimens yield lower T_0 values than those obtained from conventional specimens (i.e., non-conservative), while in other cases, they correspond to higher T_0 values (i.e., conservative). With these observations in mind and considering the data from the literature review [28], it becomes evident that structural steels follow a similar trend to the nuclear grades. However, the deviation in T_0 values for structural steels (positive or negative, depending on the particular case) tends to be greater than that observed in the nuclear materials. In any case, further evidence would be necessary to support that statement since this study is limited to four structural steels.

3.2. *Fractographical analysis*

In order to evaluate the fulfillment of the weakest link statistics in mini-C(T) specimens, which is a basic assumption for the utilization of the three-parameter Weibull distribution on which the MC is based, the fracture process must be caused by cleavage (a brittle micromechanism) and initiated from a single point (the weakest link). Cases involving multiple initiation points, while still indicative of brittle processes, do not align with the principles of the weakest link theory. Such scenarios are typically observed, for example, in fracture processes within the lower shelf of ferritic-pearlitic steels [29].

Therefore, the aim of this analysis is to determine whether the mini-C(T) specimens tested within the experimental program experienced cleavage fracture associated with a single initiation site. With this aim, the fracture surfaces of all tested specimens were examined by means of a scanning electron microscope (SEM). The analysis consisted in three steps: 1) a general view of the two broken halves, 2) a detailed examination of the fracture surface of one half, and 3) a detailed inspection of the fracture initiation site at 500x

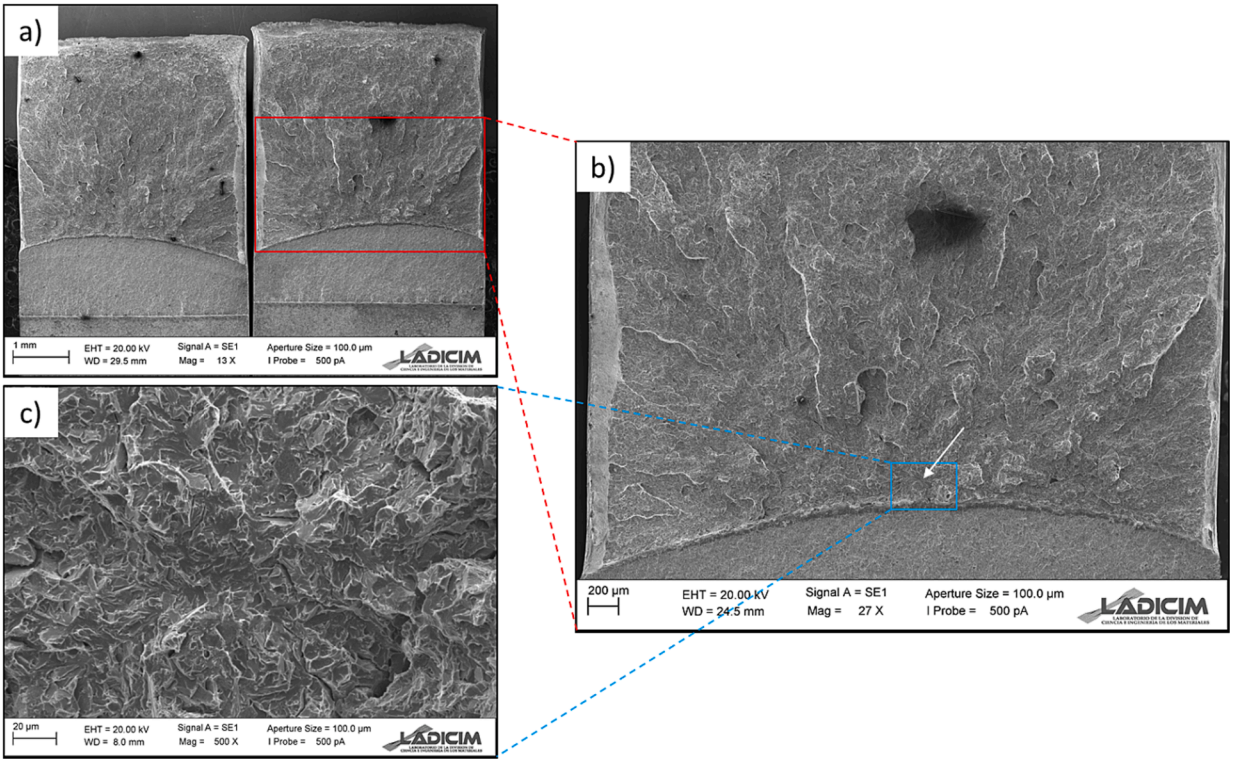

Fig. 16. SEM analysis of S690Q_11 specimen (T = -100 °C / $K_{Jc,0.16T}$ = 126 MPa$\sqrt{m}$): a) overview of the two halves; b) crack front and fracture surface; c) detail of the initiation area.

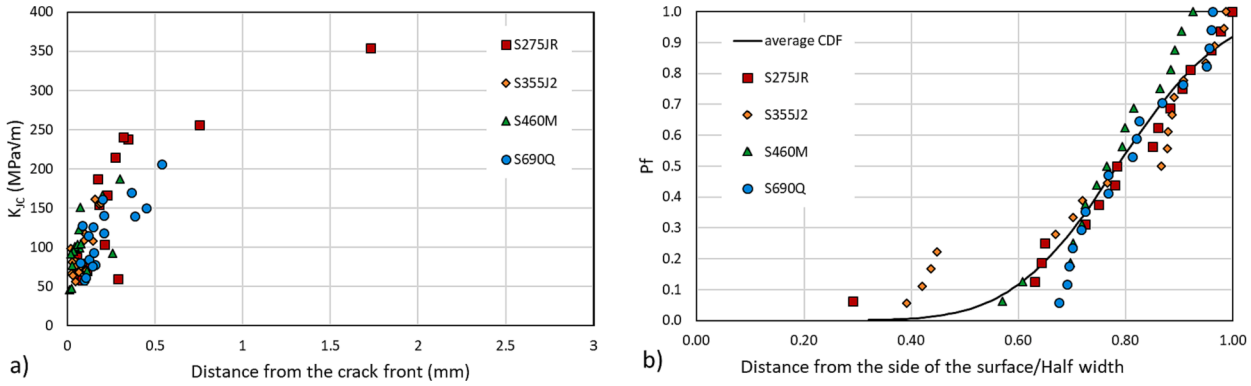

Fig. 17. A) fracture toughness results vs distance between the initiation site and the crack tip; b) cumulative initiation location distribution.

magnification.

Figs. 13 to 16 present examples of the fracture surfaces observed in one specimen from each material, captured at varying magnifications, with special emphasis on identifying the most likely initiation zone. These examples were selected because their K_{Jc} values were non-censored, and their test temperatures were close to the T_0 value, but analogous observations were made in all cases.

In the four structural steels analyzed in this study, the majority of the fracture surfaces exhibited initial crack fronts with very narrow or non-existent ductile tearing areas (typically between zero and a few microns). After such limited ductile tearing, if any, or immediately beyond the front of the fatigue pre-crack, cleavage fracture was identify as the primary mode of failure in all cases. Small areas of ductile fracture were not uncommon (especially in the S275JR steel), and in a few instances, limited intergranular fracture was observed. Furthermore, some specimens presented a slant fracture area at the sides (e.g., Fig. 16a), as a consequence of the plane stress effect in that region and the fact that the specimens were not side-grooved.

In each case, a single initiation point was identified, or at the very least, a clearly predominant initiation area. The distances from the crack front as well as from the side surfaces were measured as soon as the primary fracture initiation side was located. Fig. 17a

illustrates the relation between the fracture toughness values and the distance between the identified initiation site and the crack tip. Initiation sites located at greater distances from the crack front are clearly associated to higher K_{Jc} values. This phenomenon is not specific to mini-C(T) specimens and occurs because, when the initiation site (or triggering site) is located further from the crack front, the required critical stress at such location corresponds to higher external forces (the stress field relaxes moving away from the crack front) and, consequently, larger toughness values are developed [12].

Fig. 17b shows the cumulative distribution of the initiation locations. The data indicates that most of the initiation points were often located close to the middle of the specimen, where triaxiality conditions are maximum. Specifically, the majority of initiations are concentrated in the central 40 % of the specimens. This observation aligns with the findings of the study conducted by Wallin on both conventional and mini-C(T) specimens [27].

In summary, the SEM analyses unequivocally support the conclusion that the fracture process in the mini-C(T) specimens examined in this study followed the weakest link theory and are comparable to those observed in conventional specimens. Cleavage fracture was the governing micromechanism, with a single initiation site triggering the entire fracture process.

4. Conclusions

This study investigated and validated the use of mini-C(T) specimens to determine the Master Curve (MC) of four distinct structural steel grades: S275JR, S355J2, S460M, and S690Q. The key findings and conclusions drawn from this investigation are as follows:

- Reference temperature (T_0) were successfully obtained using mini-C(T) specimens for all materials. The resulting Master Curves provide a good representation of their fracture toughness in the ductile-to-brittle transition region.
- The comparison between the T_0 values obtained using mini-C(T) specimens and those obtained through conventional specimens reveals that the differences generally fall within of $\pm$ 30 °C, with positive and negative deviations depending on the specific case. In other words, no consistent tendency towards conservatism or non-conservatism has been observed.
- The predictions are in agreement with those obtained over the years on both non-irradiated and irradiated nuclear grades, although in the case of the structural steels it has been observed that the difference between the T_0 values derived from mini-C(T) specimens and the T_0 values derived from conventional specimens could tend to be larger. Further research and additional tests on other steels are required to confirm the trends obtained here.
- The analysis of fracture micromechanisms observed on mini-C(T) specimens reveal that the MC assumptions are met when using this type of geometry, as the fracture process adheres to the principles of weakest link statistics, with a single initiation point triggering the cleavage process.

CRediT authorship contribution statement

Marcos Sánchez: Writing – original draft, Methodology, Investigation, Formal analysis, Data curation, Conceptualization. **Sergio Cicero:** Writing – review & editing, Methodology, Investigation, Funding acquisition, Conceptualization. **Borja Arroyo:** Writing – review & editing, Investigation, Data curation.

Declaration of competing interest

The authors declare the following financial interests/personal relationships which may be considered as potential competing interests: Sergio Cicero reports financial support was provided by Euratom Research and Training Programme. If there are other authors, they declare that they have no known competing financial interests or personal relationships that could have appeared to influence the work reported in this paper.

Data availability

Data will be made available on request.

Acknowledgments

This research has received funding from the Euratom research and training programme 2019-2020 under grant agreement N° 900014.

References

[1] Aldazabal J, Martín-Meizoso A, Klimpel A, Bannister A, Cicero S. Mechanical and microstructural features of plasma cut edges in a 15 mm thick S460M steel plate. Metals 2018;8:447. https://doi.org/10.3390/met8060447.
[2] Sharpe WN, Danley D, LaVan DA. Microspecimen Tensile Tests of A533-B Steel. Small Specim. Test Tech. ASTM International 1998:497–512. https://doi.org/10.1520/STP38008S.
[3] Jung P, Hishinuma A, Lucas GE, Ullmaier H. Recommendation of miniaturized techniques for mechanical testing of fusion materials in an intense neutron source. J Nucl Mater 1996;232:186–205. https://doi.org/10.1016/S0022-3115(96)00394-7.

[4] Andres D, Lacalle R, Cicero S, Alvarez JA. Application of the small punch test in combination with the master curve approach for the characterisation of the ductile to brittle transition region. J Nucl Mater 2019;518:409–18. https://doi.org/10.1016/j.jnucmat.2019.03.011.
[5] Altstadt E, Bergner F, Houska M. Use of the small punch test for the estimation of ductile-to-brittle transition temperature shift of irradiated steels. Nucl Mater. Energy 2021;26. https://doi.org/10.1016/j.nme.2021.100918.
[6] Kim MC, Oh YJ, Lee BS. Evaluation of ductile-brittle transition temperature before and after neutron irradiation for RPV steels using small punch tests. Nucl Eng Des 2005;235:1799–805. https://doi.org/10.1016/j.nucengdes.2005.05.014.
[7] Sánchez M, Cicero S, Arroyo B, Cimentada A. On the use of mini-CT specimens to define the Master Curve of unirradiated reactor pressure vessel steels with relatively high reference temperatures. Theor Appl Fract Mech 2023;124:103736. https://doi.org/10.1016/j.tafmec.2022.103736.
[8] Miura N, Soneda N. Evaluation of Fracture Toughness by Master Curve Approach Using Miniature C(T) Specimens. ASME 2010 Press. Vessels Pip. Conf. Vol. 1, vol. 77, ASMEDC; 2010, p. 593–602. https://doi.org/10.1115/PVP2010-25862.
[9] Yamamoto M, Kimura A, Onizawa K, Yoshimoto K, Ogawa T, Mabuchi Y, et al. A round Robin program of master curve evaluation using miniature C(T) specimens-3RD report: Comparison of T0 under various selections of temperature conditions. Am. Soc. Mech. Eng. Press. Vessels Pip. Div. Publ. PVP, vol. 1, 2014, p. 1–7. https://doi.org/10.1115/PVP201428898.
[10] Chaouadi R, Walle EV, Scibetta M, Gérard R. On the use of miniaturized ct specimens for fracture toughness characterization of RPV materials. Am. Soc. Mech. Eng. Press. Vessels Pip. Div. Publ. PVP, vol. 1B-2016, 2016, p. 1–10. https://doi.org/10.1115/PVP2016-63607.
[11] ASTM I. ASTM E1921-21, Standard Test Method for Determination of Reference Temperature, T0, for Ferritic Steels in the Transition Range. vol. 03.01. West Conshohocken, PA, USA: ASTM International; 2021. https://doi.org/10.1520/E1921-21.
[12] Anderson TL. Fracture mechanics: fundamentals and applications. 4th ed. CRC Press; 2005.
[13] Wallin K. The scatter in KIC results. Eng Fract Mech 1984. https://doi.org/10.1016/0013-7944(84)90153-X.
[14] Wallin K. Master curve analysis of the "Euro" fracture toughness dataset. Eng Fract Mech 2002;69:451–81. https://doi.org/10.1016/S0013-7944(01)00071-6.
[15] Scibetta M, Lucon E, Walle EV. Optimum use of broken Charpy specimens from surveillance programs for the application of the master curve approach. Int J Fract 2002;116:231–44. https://doi.org/10.1023/A:1020165900918.
[16] Sokolov MA. Use of Mini-CT Specimens for Fracture Toughness Characterization of Irradiated Highly Embrittled Weld. Vol. 1 Codes Stand., American Society of Mechanical Engineers; 2022, p. 10–3. https://doi.org/10.1115/PVP2022-84827.
[17] Cicero S, García T, Madrazo V, Carrascal IA, Ruiz E. Analysis of notch effect in load bearing capacity, apparent fracture toughness and fracture micromechanisms of ferritic–pearlitic steels. Eng Fail Anal 2014;44:250–71. https://doi.org/10.1016/j.engfailanal.2014.05.007.
[18] Cicero S, García T, Madrazo V. Application and validation of the notch master curve in medium and high strength structural steels. J Mech Sci Technol 2015;29:4129–42. https://doi.org/10.1007/s12206-015-0907-2.
[19] European Committee for S. UNE-EN 10025-2:2020, Productos laminados en caliente de aceros para estructuras. Parte 2: Condiciones técnicas de suministro de los aceros estructurales no aleados. 2020.
[20] European Committee for S. UNE-EN 10025-4:2020, Productos laminados en caliente de aceros para estructuras. Parte 4: Condiciones técnicas de suministro de los aceros estructurales soldables de grano fino laminados termomecánicamente. 2020.
[21] European Committee for S. UNE-EN 10025-6:2020+A1:2023, Productos laminados en caliente de aceros para estructuras. Parte 6: Condiciones técnicas de suministro de los productos planos de aceros estructurales de alto límite elástico en la condición de templado y revenido. 2023.
[22] ASTM I. ASTM E8/E8M-13a, Standard Test Methods for Tension Testing of Metallic Materials. vol. 16. ASTM International; 2013.
[23] ASTM I. ASTM E23-12, Standard Test Methods for Notched Bar Impact Testing of Metallic Materials. vol. 03.01. ASTM International; 2012. https://doi.org/10.1520/E0023-23A.
[24] ASTM I. ASTM E1921-13, Standard Test Method for Determination of Reference Temperature, T0, for Ferritic Steels in the Transition Range. vol. 03.01. ASTM International; 2013. https://doi.org/10.1520/E1921-21.
[25] Cicero S, Madrazo V, García T, Cuervo J, Ruiz E. On the notch effect in load bearing capacity, apparent fracture toughness and fracture mechanisms of polymer PMMA, aluminium alloy Al7075-T651 and structural steels S275JR and S355J2. Eng Fail Anal 2013;29:108–21. https://doi.org/10.1016/j.engfailanal.2012.11.010.
[26] Landes JD. J calculation from front face displacement measurement on a compact specimen. Int J Fract 1980;16:R183–5. https://doi.org/10.1007/BF00018249.
[27] Wallin K, Yamamoto M, Ehrnstén U. Location of Initiation Sites in Fracture Toughness Testing Specimens: The Effect of Size and Side Grooves. Vol. 1B Codes Stand., vol. 1B-2016, American Society of Mechanical Engineers; 2016. https://doi.org/10.1115/PVP2016-63078.
[28] Sánchez M, Cicero S, Kirk M, Altstadt E, Server W, Yamamoto M. Using Mini-CT Specimens for the Fracture Characterization of Ferritic Steels within the Ductile to Brittle Transition Range: A Review. Metals 2023;13. https://doi.org/10.3390/met13010176.
[29] Wallin K. The master curve method: a new concept for brittle fracture. Int J Mater Prod Technol 1999;14:342. https://doi.org/10.1504/IJMPT.1999.036276.